UC Irvine
UC Irvine Previously Published Works

Title

Kinetics of the reactions of diatomic sulfur with atomic oxygen, molecular oxygen, ozone, nitrous oxide, nitric oxide, and nitrogen dioxide

Permalink

https://escholarship.org/uc/item/4b89w53t

Journal

The Journal of Physical Chemistry, 91(5)

ISSN

0022-3654

Authors

Hills, Alan J
Cicerone, Ralph J
Calvert, Jack G
et al.

Publication Date

1987-02-01

DOI

10.1021/j100289a033

heat flux evolution equations[17] as represented by (2.5). These investigations[16,17] indicate that the flux evolution (2.5) can give an excellent description of transport processes in fluids near or far from equilibrium. Therefore the evolution eq 2.5 are not without experimental bases, even though they are part of postulates in the present formulation of a global theory.

In the original Gibbsian theory of heterogeneous phases the device of virtual variations of thermodynamic variables is employed and what dynamically causes the virtual variations is not specified since there are no evolution equations to describe them. In the present approach such a device is not necessary and any variations in macroscopic variables causing the system to suffer displacement from equilibrium can be precisely described by their global evolution equations presented in the text. Yet we obtain exactly the same result for the phase rule for reacting systems.

The stability study made in section V gives us a mathematical means to carry out stability analysis for a macroscopic, global thermodynamic system by using the variational dynamic evolution equations for the variables involved such as E_ψ^α, V^α, etc. since such evolution equations are available in the present theory. This again is in contrast to the stability theory based on the equilibrium Gibbs relation, which is a static theory without dynamical equations for extensive variables. The analysis shows that except for the case of chemical reactions the second variation of entropy may be regarded as a Lyapounov function.

(17) Eu, B. C. *Physica* **1985,** *A133,* 120. Eu, B. C. *Phys. Fluids* **1985,** *28,* 222.

The calculation presented in section VI is for a simple illustration of application of the theory although the result obtained appears to be quite interesting. There is, of course, room for refining the model, and if we do, we may find a better irreversibility factor instead of the factor 1/2 we have obtained here. In my opinion it is significant that the efficiency of the irreversible Carnot cycle is less than unity for all values of T_2/T_1, because the irreversibility does not disappear even if T_2/T_1 is made equal to zero. If the cycle is irreversible, the efficiency should not reach that of the reversible Carnot cycle as is the case with the Curzon–Ahlborn formula. A crucial difference is in the inclusion of the dissipation Ξ of the available energy in the present calculation.

In this paper we have examined through derivation the local field theory basis of various aspects of irreversible thermodynamics of heterogeneous systems. Various derivations of formulas indicate what sort of assumptions and limitations must be imposed if one wishes to make use of suitable ad hoc generalizations of equilibrium thermodynamic formulas to nonequilibrium forms for heterogeneous systems. The present theory also provides ways to overcome the limitations, if necessary, by resorting to the various integral forms of local field variables and equations presented, since even formulas and equations that appear to be nothing new from the equilibrium thermodynamics viewpoint come with their local field theory counterpart. Therefore the present formulation can serve as a starting point for studies on macroscopic phernomena in heterogeneous systems from the molecular standpoint.

Kinetics of the Reactions of S₂ with O, O₂, O₃, N₂O, NO, and NO₂

Alan J. Hills,* Ralph J. Cicerone, Jack G. Calvert, and John W. Birks†

National Center for Atmospheric Research (NCAR), Advanced Study Program, Boulder, Colorado 80307 (Received: June 16, 1986)

Rates of the reactions $S_2 + O \rightarrow SO + S$ (10), $S_2 + O_2 \rightarrow$ products (1), $S_2 + O_3 \rightarrow$ products (18), $S_2 + N_2O \rightarrow$ products (20), $S_2 + NO \rightarrow$ products (21), $S_2 + NO_2 \rightarrow$ products (19) were investigated at 409 K and low pressure (0.89–3.0 Torr) in a discharge-flow system with mass spectrometric detection. Reaction 10 was found to be fast with $k_{10} = (1.12 \pm 0.20) \times 10^{-11}$ cm³ molecule⁻¹ s⁻¹. Under the experimental conditions, S_2 did not react with O_2, O_3, N_2O, NO, or NO_2. Upper limits for the rate constants of these reactions are $k_1 < 2.3 \times 10^{-19}$, $k_{18} < 4.0 \times 10^{-15}$, $k_{20} < 3.2 \times 10^{-17}$, $k_{21} < 8.5 \times 10^{-17}$, and $k_{19} < 1.1 \times 10^{-15}$ cm³ molecule⁻¹ s⁻¹. Reaction 10 produced a large ion current at m/e 48 leading to the conclusion that $S_2 + O$ produces $SO + S$ as primary products.

Introduction

Diatomic sulfur is emitted to the atmosphere from volcanos.[1–5] In his summary of volcanic emissions from six volcanos, Gerlach reports that the fraction of S_2 of total sulfur can be as high as 14% on a molar basis.[4] We were curious as to the possible chemical reactions of S_2 in the atmosphere. The usual fate of reduced sulfur compounds after atmospheric injection is that of oxidation.[6–8] However, a review of kinetics information for sulfur species yielded no reported rate constants for ground-state, gaseous S_2, except for an approximate value reported for $S_2 + O$.[9] Table I lists possible atmospheric reactions of S_2. These are all exothermic and have the potential for rapid reaction with S_2. If the reaction

$$S_2 + O_2 \rightarrow SO + SO \qquad (1)$$

were to occur it would dominate the atmospheric chemistry of S_2 due to the high concentration of O_2 in air (20.9%). However,

TABLE I: Some Possible Atmospheric Reactions of S₂

reaction	ΔH_{298},[a] kcal mol⁻¹
$S_2 + O \rightarrow SO + S$	−22.1
$S_2 + O_2 \rightarrow SO + SO$	−27.6
$S_2 + O_3 \rightarrow SSO + O_2$	−77.7
$S_2 + NO_2 \rightarrow SSO + NO$	−29.9
$S_2 + N_2O \rightarrow SSO + N_2$	−63.2
$S_2 + OH \rightarrow SSO + H$	−0.8
$S_2 + OH \rightarrow SO + HS$	−3.9
$S_2 + OH + M \rightarrow S_2 \cdot OH$	<−95
$S_2 + HO_2 \rightarrow SSO + OH$	−37.3[b]
$S_2 + HO_2 \rightarrow SSH + O_2$	−11.7[b]

[a] References 17, 24, and 33. [b] Reference 34.

the reaction would proceed through an unlikely four-center intermediate. The goal of this research was to measure the rate

*To whom correspondence should be addressed.
†Present address: Department of Chemistry and Biochemistry and Cooperative Institute for Research in Environmental Sciences (CIRES), Campus Box 449, University of Colorado, Boulder, CO 80309.

(1) Giggenbach, W. F. *Bull. Volcanol.* **1975,** *39,* 132.
(2) Le Guern, F.; Nohl, A.; Bicocchi, P. *Bull. Volcanol.* **1982,** *45,* 229.
(3) Gerlach, T. M. *Bull. Volcanol.* **1982,** *45,* 249.
(4) Gerlach, T. M. *Bull. Volcanol.* **1982,** *45,* 236.
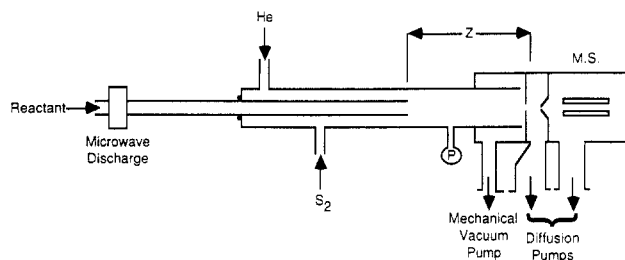(5) Gerlach, T. M. *Bull. Volcanol.* **1982,** *45,* 191.

Figure 1. Schematic diagram of the mass spectrometer flow system.

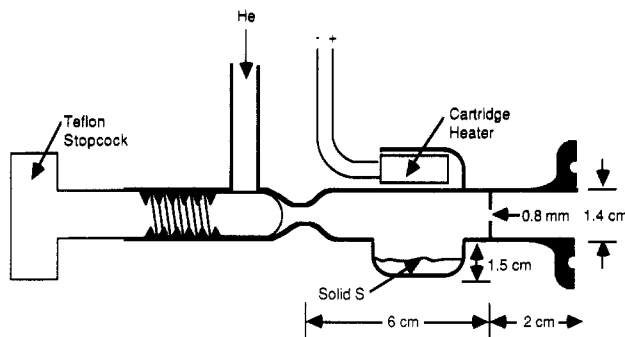**Figure 2.** Schematic diagram of the quartz S_2 source (side view).

constants for the reactions of S_2 with O, O_2, O_3, N_2O, NO, and NO_2, and to establish the reaction products where possible.

Experimental Section

Flow Tube Apparatus. The kinetics investigations were performed with the technique of discharge-flow mass spectrometry. Discharge-flow mass spectrometry[10] and the discharge flow technique in general[11] have been described previously. The system used in these experiments is shown in Figure 1. It consists of a 110-cm long, 2.51-cm i.d., Pyrex tube. S_2 is produced in a sidearm attached to this tube. Inserted into the flow tube is a 115-cm long, 1.2-cm o.d., movable inlet. The reactants O, O_2, O_3, N_2O, NO, and NO_2 were admitted through this movable tube. S_2 and another reactant mix at the exit of the injector and react for a distance z before a small fraction of the gas mixture is admitted into the ion source of a UTI (Model 100C-02) quadrupole mass spectrometer. Since the reaction distance is determined by the position of the movable injector, changing its position provides a means of altering reaction time in this system. The pressures in the flow tube, the intermediate chamber, and mass spectrometer chamber were typically 1.3, 5×10^{-4}, and 8×10^{-6} Torr, respectively. Ions were detected with a Channeltron (Model 4717) electron multiplier, operated in the analog mode. Detection limits were typically 10^{10}–10^{11} molecules cm^{-3} at S/N = 2.

Reagents. Cylinder gases used in this work were helium (UHP, >99.999%), nitric oxide (CP, >99%), oxygen (UHP, >99.97%), and nitrous oxide (CP, >99%). Nitrogen dioxide was prepared by reacting nitric oxide with oxygen. The NO_2 was further purified via trap-to-trap distillation in the presence of excess oxygen until an aliquot was a white solid at 197 K, free of any bluish N_2O_3 impurities. Excess oxygen was then removed by pumping on the solid at 197 K. Ozone was produced by electrical discharge of a slow stream of oxygen (1 STP cm^3 s^{-1}) and was used in real time in the kinetics experiments. The O_2 to O_3 conversion was typically 4%. Oxygen atoms were generated in the movable inlet via microwave discharge of O_2 at 2450 MHz. The discharge efficiency for the conversion $O_2 \rightarrow 2O$ was 5%.
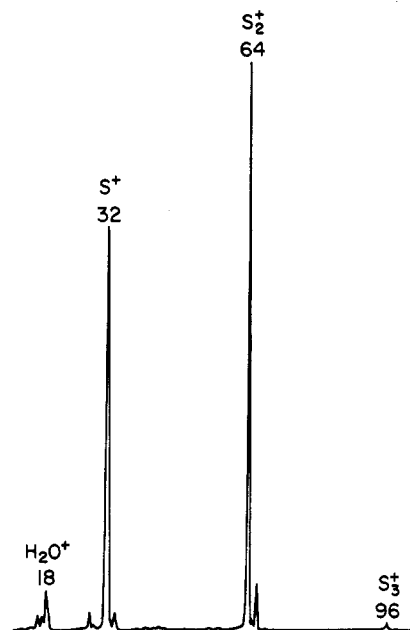

Figure 3. Mass spectrum of the S_2 source output in the range 10–110 amu, at 10^{-6} A full scale. The important ions are m/e 96, S_3^+; m/e 64, S_2^+; m/e 32, S^+.
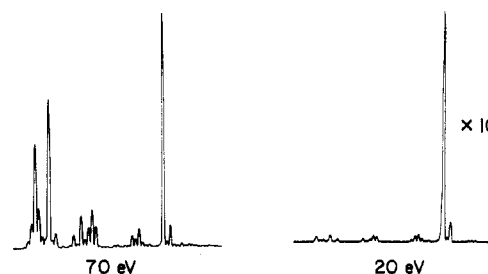

Figure 4. Mass spectra of the S_2 source output at electron impact energies of 70 (left) and 20 eV (right), magnified 10X.

S_2 Source. Diatomic sulfur was generated thermally from solid sulfur. Four different designs were used, the fourth being shown in Figure 2. This source, constructed of quartz, is heated to ≈125 °C by a small cartridge heater connected to a Variac. The proper combination of source temperature and He flow (0.20–2.3 STP cm^3/s) is adjusted so that sufficient S_2 is generated for the experiment. A typical mass spectrum of the S_2 source is shown in Figure 3. The ions observed are as follows: m/e 96, S_3^+; m/e 64, S_2^+; m/e 32, S^+; m/e 18, H_2O^+. The m/e 66 ion corresponds to $^{32}S^{34}S^+$. Higher polymers of sulfur, S_4, S_5, S_6, S_7, and S_8, were also seen at m/e 128, 160, 192, 224, and 256, respectively. These ions were seen at even much lower intensities than m/e 96. S_3^+–S_8^+ ion currents, added together, constituted less than 0.8% of the S_2^+ ion current. The fraction of higher sulfur polymers, S_3–S_8, is probably higher than 0.8%, but fragmentation of these species reduces this value. It is well-known, however, that heating of elemental sulfur at low and nonequilibrium pressures (as is the case with our source) favors the formation of S_2.[12,13] Further evidence that the source was not producing significant amounts of S_3 and higher sulfur polymers was found by passing the source effluent through a microwave discharge. This produced only a marginally greater S_2 ion current, confirming that the S_2 source does not produce significant amounts of polymeric sulfur.

The ion at m/e 32 was of concern, since it is known that S atoms are quite reactive toward the reactants used in this study.[14,15] If

(6) Graedel, T. E. *Rev. Geophys. Space Phys.* **1977**, *15*, 421.
(7) Sze, N. D.; Ko, M. K. W. *Atmos. Environ.* **1980**, *14*, 1223.
(8) Stockwell, W. R.; Calvert, J. G. *Atmos. Environ.* **1983**, *17*, 2231.
(9) Homann, K. H.; Krome, G.; Wagner, H. Gg. *Ber. Bunsen-Ges Phys. Chem.* **1968**, *72*, 998.
(10) Birks, J. W.; Shoemaker, B.; Leck, T. J.; Borders, R. A.; Hart, L. J. *J. Chem. Phys.* **1977**, *66*, 4591.
(11) Howard, C. J. *J. Phys. Chem.* **1979**, *83*, 3.

(12) Meyer, B. *Chem. Rev.* **1976**, *76*, 367.
(13) Rau, H.; Kutty, T. R. N.; Guedes de Carvalho, J. R. F. *J. Chem. Thermodyn.* **1973**, *5*, 833.
(14) "Chemical Kinetics and Photochemical Data for Use in Stratospheric Modeling", NASA Panel for Data Evaluation, Evaluation No. 7, Jet Propulsion Laboratory Publication 85-37, Pasadena, CA, 1985.
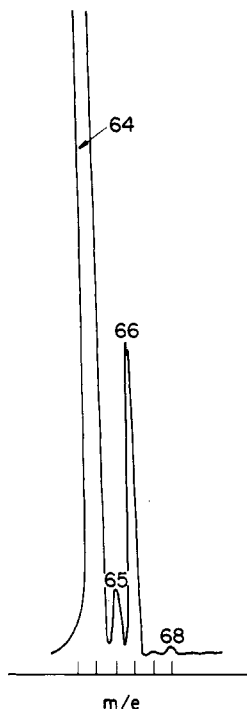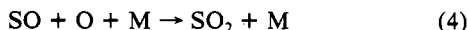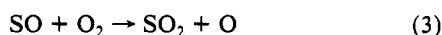
Figure 5. Mass spectrum of S$_2$ at 70-eV electron impact energy and 10^{-8} A full scale.

the S$_2$ source produced S atoms, it is possible that this highly reactive species could react with O$_2$ forming SO

$$S + O_2 \rightarrow SO + O \tag{2}$$

which conceivably could form SO$_2$

$$SO + O_2 \rightarrow SO_2 + O \tag{3}$$

$$SO + O + M \rightarrow SO_2 + M \tag{4}$$

SO$_2$ has the same nominal mass as S$_2$. Two experiments were performed that showed the S$^+$ ion at m/e 32 was in fact a mass spectrometer fragment of S$_2$ and not atomic S generated in the S$_2$ thermal source. The first test was to decrease the electron impact energy from 70 to 20 eV. At 20 eV (Figure 4) the m/e 32 peak has vanished, and the S$_2^+$ ion at m/e 64 remains. Since fragmentation decreases with decreased electron impact energy, this gives support, but does not prove that S$^+$ is an electron impact fragment of S$_2^+$. A second test was performed taking advantage of reaction 2. O$_2$ was added to the effluent of the S$_2$ source, and the ion current at m/e 48 monitored. No significant ion current could be detected, leading to the conclusion that the ion at m/e 32 is, in fact, a fragment of S$_2$ or S$_2^+$ within the ion source, most likely produced by

$$S_2 + e^- \rightarrow S^+ + S + 2e^- \tag{5}$$
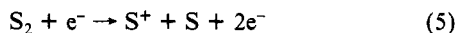
The S$_2$ source was constructed of quartz so that it could be quenched by cooling with water, thus shutting off S$_2$ rapidly. This was useful for calibration purposes. The S$_2$ source has a constant surface area of molten sulfur. Helium flow over this surface resulted in a very stable S$_2$ output with less than 5% fluctuation over 20 min.

The flow tube was kept at 409 K for all experiments, since it was found that S$_2$ wall loss approached unity at temperatures below 380 K. At 395 K, S$_2$ wall loss is essentially completely eliminated as indicated by an invariant S$_2$ signal as a function of movable inlet position. The flow tube exit housing, constructed of stainless steel, was also heated to eliminate S$_2$ surface loss which would otherwise have added to the background signal at m/e 64. An amplified mass spectrum of S$_2$ is shown in Figure 5. It clearly shows four of the isotopes of S$_2$: m/e 64, ^{32}S^{32}S; m/e 65, ^{32}S^{33}S;
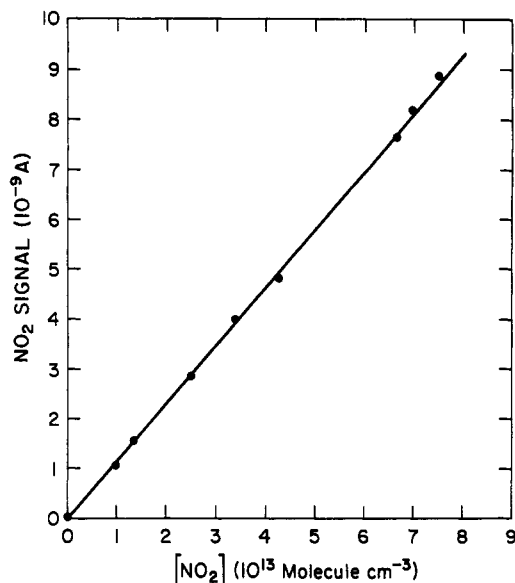
(15) Davis, D. D.; Klem, R. B.; Pilling, M. *Int. J. Chem. Kinet.* **1972**, *4*, 367.

Figure 6. Typical NO$_2$ calibration plot.

m/e 66, ^{32}S^{34}S; m/e 68, ^{34}S^{34}S. The relative intensities roughly correspond to those calculated based on the isotopic abundances of bulk sulfur.[16]

Calibrations. Flow rates of the bulk carrier gas, He, and the stable reactant gases, O$_2$, N$_2$O, and NO, were measured and controlled by mass flow controllers (Tylan FC 260 and FC 200 and Teledyne Hastings NALL-100). The meters were intercalibrated by putting identical He flows through them (as monitored by equal flow tube pressures) and observing the flow rate displayed. Two factory-calibrated Tylan FC 260 flow meters served as primary flow rate standards. NO$_2$ flow rates were measured by the technique of differential pressure change over time in a calibrated glass volume

$$F_{NO_2} = \frac{\Delta P}{\Delta t} \frac{V}{T} \left(\frac{273}{760} \right) \tag{6}$$

where F_{NO_2} represents the STP flow of NO$_2$ (cm^3 s^{-1}), ΔP is the pressure change (Torr) in time Δt, V is the volume sum of a calibrated chamber and connected lines ($V = 3520$ cm^3), and T is the absolute temperature in the calibration region. NO$_2$ flow rates were corrected for dimerization of NO$_2$

$$N_2O_4 = NO_2 + NO_2 \tag{7}$$
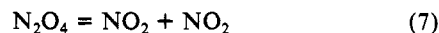
$$F_{NO_2,cor} = F_{av,meas} \left(1 + \frac{2P_{av}}{K_p} \right)$$

where P_{av} (Torr) is the average pressure in the calibrated volume, and $K_p = P_{NO_2}^2/P_{N_2O_4}$ is the equilibrium constant for NO$_2$ dimerization ($K_{p,298} = 106$ Torr).[17] The correction made to NO$_2$ flows to account for dimerization ranged from 1.0 to 2.2%.

Ozone concentrations were measured by reaction with excess NO

$$O_3 + NO \rightarrow O_2 + NO_2 \tag{8}$$

Since excess NO was used, and conditions were adjusted for complete conversion of O$_3$, the [NO$_2$] produced was equal to the initial [O$_3$]. The NO$_2$ thus formed was monitored at m/e 46. Dividing this ion current by the slope of an NO$_2$ mass spectrometer signal vs. [NO$_2$] plot (Figure 6) yields the initial concentration of ozone. NO$_2$ calibrations were performed one or two times daily.

(16) Weast, R. C.; Astle, M. J. *Handbook of Chemistry and Physics*, CRC Press: Boca Raton, FL, 1981–1982; 62nd ed, p B-260.

(17) Unless otherwise noted, all thermochemical data are from *JANAF Thermochemical Tables*, Stull, D. R., Prophet, H., Ed.; National Bureau of Standards: compiled and calculated by the Dow Chemical Co., Midland, MI, including revised tables issued through 1982.
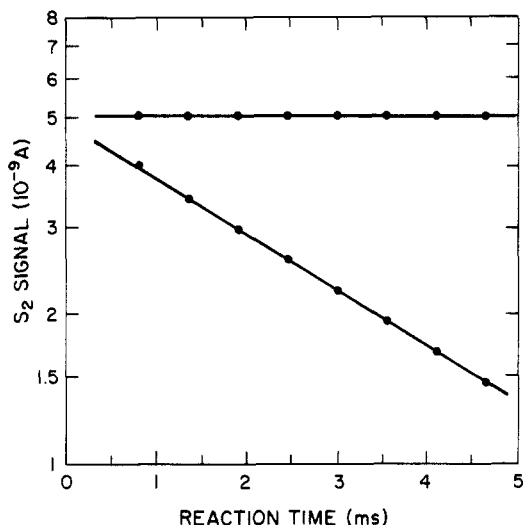
Figure 7. Typical kinetics data for the S_2 + O reaction. The upper plot is the variation in S_2 ion current as a function of movable inlet position with the O source turned off. The lower plot shows the decrease in S_2 signal as a function of injector position in the presence of excess atomic O. Note that reaction time is directly proportional to injector position, since the linear flow velocity is known.

The concentration of oxygen atoms was measured in a similar manner by using the reaction

$$O + NO_2 \rightarrow O_2 + NO \qquad (9)$$

When measuring the O atom concentration, conditions were adjusted so that NO_2 was in excess of O. With conditions also set so that >99% of O was consumed, the microwave discharge of oxygen was alternately turned on and off, and the ΔNO_2 signal at m/e 46 was used in conjunction with the NO_2 calibration plot (Figure 6) to arrive at [O].

Flow tube pressure was monitored with a capacitance manometer (MKS Baratron Model 170M). This was calibrated by referencing to an identical Baratron which was factory calibrated during this study. Temperatures were measured with copper/constantan thermocouples referenced to 0 °C (ice water). The 1-in. nominal Pyrex flow tube was measured internally at several points with a telescoping micrometer. The average internal diameter was found to be 0.987 in. (2.51 cm).

The inner surface of the movable injector was coated with phosphoric acid to obtain higher O atom fluxes into the flow tube. No other surfaces were coated in this study. O atom losses along the length of the flow tube were measured by titration using reaction 9, this time introducing NO_2 through a port at the exit of the flow tube. ΔNO_2 did not vary with injector position, indicating negligible wall loss of O atoms.

Results

S_2 + O Absolute Method. All of the kinetics measurements were made under pseudo-first-order conditions, $[O]_0 \gg [S_2]_0$. This condition was checked primarily by observing the linearity of pseudo-first-order decay plots. A typical decay plot for the reaction

$$S_2 + O \rightarrow products \qquad (10)$$
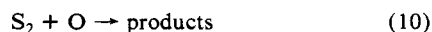
is shown in Figure 7. The reaction distance was varied 20 cm. Over this distance the $[S_2]$ decreased by about a factor of 3. The upper plot shows S_2 measurements taken with the O discharge turned off. This blank is performed to account for any S_2 destruction due to

$$S_2 + injector\ surface \rightarrow products \qquad (11)$$
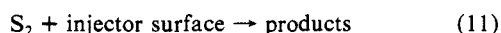
At 409 K the slope of this plot is 0.0 ± 0.1 s⁻¹, indicating no S_2 surface loss. The lower plot shows the change in S_2 signal as a function of increasing O + S_2 reaction time. Usually, two or more S_2 decays were recorded before the [O] was measured. The average of the slopes of the two S_2 decays was used to calculate

TABLE II: Data Summary for the Reaction S_2 + O → SO + S (at 409 K and 0.89–1.60 Torr)

no. of measurements	method	$k,{}^a$ 10^{-11} cm³ molecule⁻¹ s⁻¹
24	absolute: P, T, flow rates, z, [O]	1.10 ± 0.13^b
9	relative: $k = k_{O+NO_2}\left[\dfrac{\left(\dfrac{d \ln [S_2]}{dt}\right)_{O+S_2}}{\left(\dfrac{d \ln [NO_2]}{dt}\right)_{O+NO_2}}\right]$	1.19 ± 0.17^b

^{a} Recommended value: $(1.12 \pm 0.20)^c \times 10^{-11}$ cm³ molecule⁻¹ s⁻¹. ^{b} The error represents one standard deviation of the raw data. ^{c} The error is a combination of b and an estimate of systematic errors.

k^1 for a particular concentration of O. If the slope of ln $[S_2]_t$ vs. time plots for consecutive S_2 decays differed by >5%, the data were discarded. The bimolecular rate constant was extracted by using the equation

$$k = \frac{k^1}{[O]} \qquad (12)$$

Twenty-four measurements of reaction 10 were made by the absolute method with the average, $k_{10} = (1.10 \pm 0.12)\ 10^{-11}$ cm³ molecule⁻¹ s⁻¹.

A linear regression performed on k^1 vs. [O] data yielded an intercept of −17 s⁻¹ and a slope of 1.14×10^{-11} cm³ molecule⁻¹ s⁻¹. However, due to the relatively narrow range in excess reactant concentration used, $[O] = 1.77 \times 10^{13}$–$2.8 \times 10^{13}$ molecules cm⁻³, the average of the single point measurements were preferred for the absolute rate constant measurement of reaction 10. The results of these experiments are summarized in Table II.

S_2 + O Relative Method. This measurement of k_{10} was performed again using excess O atoms, but with this method an O + S_2 decay was referenced against an O + NO_2 decay, measured with the same [O] under the identical pressure and flow conditions. k_{10} was obtained by taking the ratio of the logarithms of the S_2 and NO_2 decays in the presence of a constant and large excess of [O]. This ratio was then multiplied by the recommended rate constant for O + NO_2

$$k = k_{O+NO_2}\left[\frac{\left(\dfrac{d \ln [S_2]}{dt}\right)_{O+S_2}}{\left(\dfrac{d \ln [NO_2]}{dt}\right)_{O+NO_2}}\right] \qquad (13)$$

where $k_{O+NO_2} = 9.3 \times 10^{-12}$ cm³ molecule⁻¹ s⁻¹.[14,18] The value of k_{10} was measured nine times by this method. The average, reported in Table II, is $k_{10} = (1.19 \pm 0.17) \times 10^{-11}$ cm³ molecule⁻¹ s⁻¹. Relative rate constant measurements provide a check on possible systematic errors present in a kinetics system and add to the confidence level placed on a new rate constant. The reaction

$$O + NO_2 \rightarrow O_2 + NO \qquad (14)$$
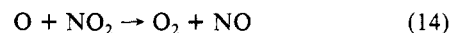
is a particularly suitable reference for this study, since it involves atomic O and as a key stratospheric reaction, it has been studied extensively.[14,18,19]

Reactions of S_2 with O_2, O_3, N_2O, NO and NO_2. No reaction was observed for S_2 with O_2, O_3, N_2O, NO, or NO_2. However, upper limits for these reactions may be established. The integrated rate equation for S_2 + A, where A is the reactant in excess is

$$\ln \frac{[S_2]_z}{[S_2]_0} = -k[A]\frac{z}{v} \qquad (15)$$

(18) Ongstad, A. P.; Birks, J. W. *J. Chem. Phys.* **1984**, *81*, 3922.

(19) Bemand, P. P.; Clyne, M. A. A.; Watson, R. T. *J. Chem. Soc. Faraday Trans. 2* **1973**, *70*, 564.

TABLE III: Upper Limits to Rate Constants for Reactions of S$_2$

reaction	k, cm^3 molecule^{-1} s^{-1}
S$_2$ + O$_2$ → products	<2.3 × 10^{-19}
S$_2$ + O$_3$ → products	<4.0 × 10^{-15}
S$_2$ + NO$_2$ → products	<1.1 × 10^{-15}
S$_2$ + N$_2$O → products	<3.2 × 10^{-17}
S$_2$ + NO → products	<8.5 × 10^{-17}
S$_2$ + NO + NO → products	<2.3 × 10^{-32}

where z is the reaction distance and v is the linear flow velocity. The smallest change in S$_2$ that would have been observed had there been reaction is used in ratioing [S$_2$]$_z$ to [S$_2$]$_0$. The relative change in S$_2$ level that was measurable was typically 1 part in several hundred. Using some actual data taken for the reaction of S$_2$ with O$_2$ (reaction 1) as an example and substituting into eq 15, one obtains

$$\ln \frac{[7.43 \times 10^{-8} \text{ A}]_{50cm}}{[7.43 \times 10^{-8} \text{ A}]_0} = -k_1[5.46 \times 10^{16}]\left[\frac{50 \text{ cm}}{473 \text{ cm/s}}\right] \quad (16)$$

Next, the upper limit for k_1 is calculated by forcing the S$_2$ ratio to change by the smallest amount that would have been easily observable had the S$_2$ signal varied (in this case 0.01 × 10^{-8} A):

$$\ln \frac{[7.42 \times 10^{-8} \text{ A}]_{50cm}}{[7.43 \times 10^{-8} \text{ A}]_0} < -k_1[5.46 \times 10^{16}]\left[\frac{50 \text{ cm}}{473 \text{ cm/s}}\right] \quad (17)$$

Therefore the upper limit for the rate constant for reaction of S$_2$ with O$_2$ is 2.3 × 10^{-19} cm^3 molecule^{-1} s^{-1}. Measured upper limits for reactions 1 and 18–21 are presented in Table III.

Discussion

The rate constant data presented in Tables II and III represent essentially the first kinetics measurements for gaseous S$_2$. The rate constant we report for reaction 10 is k_{10} = (1.12 ± 0.20) ×
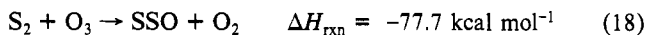
$$S_2 + O \rightarrow SO + S \quad (10)$$

10^{-11} cm^3 molecule^{-1} s^{-1}. This value is an average of the 24 absolute measurements of k_{10} and the 9 relative measurements. In a study of the reaction S + O$_2$ → SO + O, Homann et al.[9] used reaction 10 as a source of S atoms. In order to ensure completion of their sulfur atom source they briefly investigated the S$_2$ + O reaction. Their experiment involved no absolute calibration for S$_2$, their reactant in excess, and they quote only an "order of magnitude" value (at 1050 K), $k_1 \approx 4 \times 10^{12}$ cm^3 mol^{-1} s^{-1} (7 × 10^{-12} cm^3 molecule^{-1} s^{-1}). Considering the uncertainties in their work, this is in agreement with the more accurate value reported here.

An estimate of the accuracy of the rate constant measurement is derived from a consideration of both random errors associated with the raw data and possible systematic errors. The statistical error in the data for S$_2$ + O is 0.15 × 10^{-11} cm^3 molecule^{-1} s^{-1}. This represents one standard deviation for the measurements of k_1. Systematic errors are also incorporated into the overall uncertainty associated with k_1. These consist of measurement of gas flow rates (±3%), temperature (±1%), pressure (±2%), flow tube area (±2%), reaction distance (±3%), and O atom concentration (±10%). These errors yield a total systematic uncertainty of ±11.3%. Combining this with the statistical error, as the square root of the sum of the squares, a total uncertainty of 17.7% or 0.20 × 10^{-11} cm^3 molecule^{-1} s^{-1} is obtained.

The effects of axial and radial diffusion were estimated by first calculating the diffusion coefficient, $D_{S_2/He}$, for S$_2$ in He using the method of Fuller et al.[20] With $(D_{S_2/He})_{409K,1.3Torr}$ = 516 cm^2 s^{-1}, the effects of axial and radial diffusion on the measurement of k_{10} were found to be unimportant. Therefore, no corrections

were made to k_{10} to account for diffusional effects.

It is interesting that the reactions of S$_2$ which could form SSO

$$S_2 + O_3 \rightarrow SSO + O_2 \quad \Delta H_{rxn} = -77.7 \text{ kcal mol}^{-1} \quad (18)$$

$$S_2 + NO_2 \rightarrow SSO + NO \quad \Delta H_{rxn} = -29.9 \text{ kcal mol}^{-1} \quad (19)$$

$$S_2 + N_2O \rightarrow SSO + N_2 \quad \Delta H_{rxn} = -63.2 \text{ kcal mol}^{-1} \quad (20)$$

do not occur to any detectable extent. These are highly exothermic and would result in fairly stable products. SSO, disulfur monoxide, exists in both gaseous and condensed states and is a known biochemical intermediate.[21] N$_2$O is usually quite unreactive, so its lack of reaction with S$_2$ is not surprising. Reacting S$_2$ with high levels of O$_3$ (>10^{14} molecules cm^{-3}), NO$_2$ (>10^{15} molecules cm^{-3}), and N$_2$O (>10^{15} molecules cm^{-3}), under slow flow conditions showed no indication of either S$_2$ decay as a function of reaction time nor any SSO$^+$ production at m/e 80. Since SSO$^+$ might fragment under normal mass spectrometer operating conditions (e$^-$ impact energy = 70 eV), the electron impact energy was decreased to 20 eV in some experiments, but no significant m/e 80 ion current could be measured.
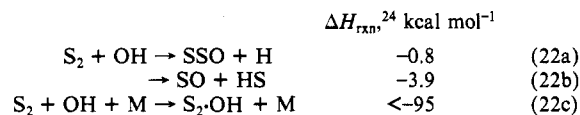
The reaction of S$_2$ with oxygen

$$S_2 + O_2 \rightarrow SO + SO \quad \Delta H_{rxn} = -27.6 \text{ kcal mol}^{-1} \quad (1)$$

although highly exothermic, was not observed—probably because the strong O$_2$ bond (BE = 119 kcal mol^{-1}) would have to be broken, and the reaction would have to proceed through an unlikely four-center intermediate. Such reactions tend to be slow or nonexistent.[22]

A study of the reaction of S$_2$ with NO was attempted to see if S$_2$ might form an adduct with NO and then disproportionate as has been proposed in the Bodenstein reaction[23]

$$S_2 + NO + M = S_2 \cdot NO + M \quad (21a)$$

$$S_2 \cdot NO + NO \rightarrow SNO + SNO \quad (21b)$$
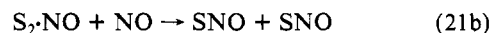
The net reaction would be first order in S$_2$ and second order in NO. No reaction was observed for S$_2$ + NO.

It is also possible that S$_2$ could react with two other common atmospheric oxidants, the hydroxl and hydroperoxyl radicals. Possible exothermic reactions with OH are

ΔH_{rxn},[24] kcal mol^{-1}

S$_2$ + OH → SSO + H	−0.8	(22a)
→ SO + HS	−3.9	(22b)
S$_2$ + OH + M → S$_2$·OH + M	<−95	(22c)

Reaction 22a is similar to reactions 18, 19, and 20 in that the S$_2$ adduct, SSO, would be formed. Since these reactions, which are much more exothermic, did not occur, reaction 22a also might not. Reaction 22b involves another four-center intermediate and is probably slow. Addition of OH to S$_2$, reaction 22c, may occur at the high pressures of the troposphere. Possible exothermic reactions of S$_2$ with HO$_2$ are

ΔH_{rxn},[24] kcal mol^{-1}

S$_2$ + HO$_2$ → SSO + OH	−37.3	(23a)
→ SSH + O$_2$	−11.7	(23b)
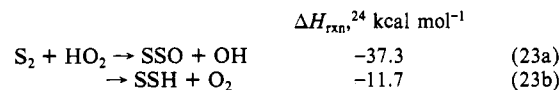
Reaction 23a is highly exothermic but would involve the formation of SSO as well as the generally poor leaving group, OH. The reaction of S$_2$ with OH and HO$_2$ merit investigation in any further study on the kinetics of S$_2$.

Analysis of Possible Interfering Reactions. The following series of reactions occur to varying extents in the S$_2$ + O reaction system:

(20) Fuller, E. N.; Schettler, P. D.; Giddings, J. C. *Ind. Eng. Chem.* **1966**, *58*, 19.

(21) Iverson, W. P. *Science* **1967**, *156*, 1112.

(22) "Proceedings of the NATO Advanced Study Institute of Atmospheric Ozone", U.S. Department of Transportation, Report No. FAA-EE-80-20 **1979**, 449.

(23) Bodenstein, M. *Z. Elektrochem.* **1918**, *24*, 183.

(24) Benson, S. W. *Chem. Rev.* **1978**, *78*, 23.

(25) Black, G.; Sharpless, R. L.; Slanger, T. G. *Chem. Phys. Lett.* **1982**, *93*, 598.

(26) Cobos, C. J.; Hippler, H.; Troe, J. *J. Phys. Chem.* **1985**, *89*, 1778.

rate constants (at 409 K)

$S_2 + O \rightarrow SO + S$	1.12×10^{-11}	(10)
$S + O_2 \rightarrow SO + O$	2.3×10^{-12} (ref 14, 15)	(2)
$SO + O_2 \rightarrow SO_2 + O$	7.3×10^{-16} (ref 14, 25)	(3)
$SO + O + M \rightarrow SO_2 + M$	5.1×10^{-31} (ref 26)	(4)
$SO + O_2(^1\Delta_g) \rightarrow SO_2 + O$	— — —	(24)

Reactions 2, 3, 4, and 24 represent possible chemical complications, interfering with the measurement of the rate constant for reaction 10. According to our product distribution estimate, $S_2 + O$ produces exclusively $SO + S$. Every S atom released in this system reacts (according to reaction 2) with O_2 forming $SO + O$. Some of this SO then forms SO_2 via reactions 3 and 4. This is a concern, since SO_2 detected as m/e 64 would be largely indistinguishable from S_2^+, also at m/e 64. Any change in the ion current at m/e 64 not due to S_2 loss as a function of increasing reaction distance with O will lead to an error in the measurement of k_{10}. However, reaction 3 is too slow to perturb significantly the m/e 64 ion current in this study; since $[O_2] = 2.6 \times 10^{14}$ molecules cm^{-3}, $k^1_{3,409K} = 0.2$ s^{-1}. The effect of reaction 4 is also quite small. Under the conditions employed here, $[O] = (1.77-2.8) \times 10^{13}$ molecules cm^{-3} and $k^1_4 = 0.4$ s^{-1}. These pseudo-first-order rate constants can be compared to the pseudo-first-order rate constants obtained for reaction 10, 169–338 s^{-1}. Nevertheless, at long reaction times the linear S_2 decay plot shown in Figure 7 would begin to flatten out as the SO_2 contribution to m/e 64 due to reaction 4 becomes significant. No corrections for SO_2 production were applied to the raw $S_2 + O$ data because of the extremely small magnitudes of these effects and the fact that they are significant only at long reaction times.

The reaction of SO with electronically excited oxygen, $O_2(^1\Delta_g)$, is energetically possible, $\Delta H_{rxn} = -35.1$ kcal mol^{-1}, but $O_2(^1\Delta_g)$ is known to be kinetically quite unreactive. An upper limit estimate of the magnitude of SO_2 production from reaction 24 can be calculated by multiplying the fastest $O_2(^1\Delta_g)$ rate constant available, that for $O_2(^1\Delta_g) + H \rightarrow OH + O,^{27}$ $k = 2.5 \times 10^{-14}$ cm^3 molecule^{-1} s^{-1}, by an expected maximum $O_2(^1\Delta_g)$ concentration. A large estimate for $O_2(^1\Delta_g)$ yield in microwave discharge of O_2/He is about 6%, which corresponds to an $O_2(^1\Delta_g)$ level of 1.6×10^{13} molecules cm^{-3} in the flow tube. The resulting pseudo-first-order rate constant for SO_2 production, $k^1_{SO+O_2(^1\Delta_g)} = 0.40$ s^{-1}. Therefore, under the conditions employed in these experiments, the effect of reaction 24 should be negligible.

Atmospheric Lifetime of S_2. If one takes the rate constant for the $S_2 + O$ reaction and an estimated value for the diurnally averaged [O] in the troposphere of 2×10^3 molecules cm^{-3}, an atmospheric lifetime of S_2 of 517 days is calculated. This chemical loss of S_2 would not significantly compete with atmospheric S_2 loss due to dry deposition. Assuming that S_2 is well mixed in the troposphere and that it has the fairly large deposition velocity of 1 cm/s, the deposition lifetime of S_2 is calculated to be 20 days. S_2 may also be lost via incorporation into aerosol droplets. This lifetime is ≈ 100 days assuming a sticking coefficient of 10^{-4}–10^{-5}. Thus, dry deposition is likely the dominant loss process for S_2 in the troposphere.

If S_2 were injected directly into the stratosphere, as with many volcanic eruptions,[28-31] the chemical lifetime of S_2 would be considerably shorter because of higher O atom concentrations. The lifetime of S_2 in the stratosphere due to reaction with O varies markedly with altitude because of the changing [O], $\tau_{S_2,25km} = 1.9$ h, $[O] = 1.3 \times 10^7$ molecules cm^{-3}; $\tau_{S_2,45km} = 25$ s, $[O] = 3.7 \times 10^9$ molecules cm^{-3}.[32] At these altitudes, photolysis of S_2 must also be considered. The S_2 bond energy of 101 kcal mol^{-1} requires wavelengths of <283 nm for photolysis. A photolysis lifetime of S_2 in the stratosphere has not been calculated, but it may be of the same order of magnitude as the chemical lifetime.

It should be pointed out that the upper limit placed on reaction 1, $k_1 < 2.3 \times 10^{-19}$ cm^3 molecule^{-1} s^{-1}, is not small enough to rule out its importance in determining the atmospheric lifetime of S_2. If the reaction of $S_2 + O_2$ were to proceed at the upper limit value for this reaction, the lifetime of S_2 would be very short, $\tau_{S_2} = 0.8$ s, due to the high atmospheric concentration of O_2 (20.9% or 5.15×10^{18} molecules cm^{-3}).

One final point can be made with regard to the atmospheric fate of S_2 due to reactions 10, 2, and 3 discussed above. The SO and S products of reaction 10 would react further in the atmosphere. S would rapidly become SO as a result of reaction 2. This SO, as well as the SO primary product, would rapidly be converted to SO_2 via reaction 3. One S_2 molecule would lead to the formation of two SO_2 molecules. Stratospheric photolysis of S_2 would also result in the formation of two SO_2 molecules. The resulting SO_2 produced from these processes would undergo subsequent chemical transformations common to atmospheric SO_2, ultimately leading to sulfuric acid, H_2SO_4.

(27) Schmidt, C.; Schiff, H. I. *Chem. Phys. Lett.* **1973**, *23*, 339.

(28) Mankin, W. G.; Coffey, M. T. *Science* **1984**, *226*, 170.
(29) Cadle, R. D. *J. Geophys. Res.* **1975**, *80*, 1650.
(30) Cicerone, R. J. *J. Geophys. Res.* **1975**, *80*, 3911.
(31) Cadle, R. D. *Rev. Geophys. Space Phys.* **1980**, *18*, 746.
(32) Brasseur, G.; Solomon, S. *Aeronomy of the Middle Atmosphere*; Reidel: New York, 1984; p 211.
(33) Berkowitz, J.; Eland, J. H. D.; Appelman, E. H. *J. Chem. Phys.* **1977**, *66*, 2183.
(34) Hills, A. J.; Howard, C. J. *J. Chem. Phys.* **1984**, *81*, 4458.